

A geometrical model for the catalogs of galaxies

L. Zaninetti

Dipartimento di Fisica Generale,
Via Pietro Giuria 1,
10125 Torino, Italy

October 29, 2021

The 3D network originated by the faces of irregular Poissonian Voronoi Polyhedrons may represent the backbone on which the galaxies are originated. As a consequence the spatial appearance of the catalogs of galaxies can be reproduced. The selected catalogs to simulate are the 2dF Galaxy Redshift Survey and the Third Reference Catalog of Bright Galaxies. In order to explain the number of observed galaxies for a given flux/magnitude as a function of the redshift, the photometric properties of the galaxies should be carefully examined from both the astronomical and theoretical point of view. The statistics of the Voronoi normalized volume is modeled by two distributions and the Eridanus super-void is identified as the largest volume belonging to the Voronoi Polyhedron. The behavior of the correlation function for galaxies is simulated by adopting the framework of thick faces of Voronoi Polyhedrons on short scales, while adopting standard arguments on large scales.

1 Introduction

During the last thirty years the spatial distribution of galaxies has been investigated from the point of view of geometrical and physical theories. One first target was to reproduce the two-point correlation function $\xi(r)$ for galaxies which on average scales as $\approx (\frac{r}{5.7Mpc})^{-1.8}$, see Jones et al. (2005) and Sparke & Gallagher (2000). The statistical theories of spatial galaxy distribution can be classified as

- **Levy flights:** the random walk with a variable step length can lead to a correlation function in agreement with the observed data, see Mandelbrot (1975), Soneira & Peebles (1977), Soneira & Peebles (1978) and Peebles (1980).
- **Percolation:** the theory of primordial explosions can lead to the formation of structures, see Charlton & Schramm (1986) and Zaninetti & Ferraro (1990). Percolation is also used as a tool to organize : (i) the mass and galaxy distributions obtained in 3D simulations of cold dark matter (CDM) and hot dark matter (HDM), see Klypin & Shandarin (1993), (ii) the galaxy groups and clusters in volume-limited samples of the Sloan Digital Sky Survey (SDSS), see Berlind et al. (2006)

The geometrical models are well represented by the **Voronoi Diagrams**. The applications to galaxies started with Icke & van de Weygaert (1987), where a sequential clustering process was adopted in order to insert the initial seeds, and they continued with van de Weygaert & Icke (1989), Pierre (1990), Barrow & Coles (1990), Coles (1991), van de Weygaert (1991), van de Weygaert (1991), Subba Rao & Szalay (1992), Ikeuchi & Turner (1991) and Goldwirth et al. (1995). An updated review of the 3D Voronoi Diagrams applied to cosmology can be found in van de Weygaert (2002) or van de Weygaert (2003). The 3D Voronoi tessellation was first applied to identify groups of galaxies in the structure of a super-cluster, see Ebeling & Wiedenmann (1993), Bernardeau & van de Weygaert (1996), Schaap & van de Weygaert (2000), Marinoni et al. (2002), Melnyk et al. (2006), van de Weygaert & Schaap (2009) and Elyiv et al. (2009). The physical models that produce the observed properties of galaxies are intimately related, for example through the Lagrangian approximation, and can be approximately classified as

- **Cosmological N-body:** Through N-body experiments by Aarseth (1978) it is possible to simulate groups which are analogous to the studies of groups among bright Zwicky-catalog galaxies, see Turner et al. (1979) or covariance functions in simulations of galaxy clustering in an expanding universe which are found to be power laws in the nonlinear regime with slopes centered on 1.9 Gott et al. (1979). Using gigaparticle N-body simulations to study galaxy cluster populations in Hubble volumes, Evrard et al. (2002) created mock sky surveys of dark matter structure to $z = 1.4$ over $10000^\circ \text{ sq. deg}$ and to $z = 0.5$ over two full spheres. In short, N-body calculations seek to model the full nonlinear system by making discrete the matter distribution and following its evolution in a Lagrangian fashion, while N-body simulations are usually understood to concern gravity only.
- **Dynamical Models:** Starting from a power law of primordial inhomogeneities it is possible to obtain a two-point correlation function for galaxies with an exponent similar to that observed, see Peebles (1974a,b); Gott & Rees (1975).

Another line of work is to assume that the velocity field is of a potential type; this assumption is called the Zel'dovich approximation, see Zel'dovich (1970); Shandarin & Zel'dovich (1989); Sahni & Coles (1995). The Zel'dovich formalism is a Lagrangian approximation of the fully nonlinear set of equations. In this sense it is “gravity” only and does not include a pressure term.

- **The halo models:** The halo model describes nonlinear structures as virialized dark-matter halos of different mass, placing them in space according to the linear large-scale density field which is completely described by the initial power spectrum, see Neyman & Scott (1952); Scherrer & Bertschinger (1991); Cooray & Sheth (2002). Figure 19 in Jones et al. (2005), for example, reports the exact nonlinear model matter distribution compared with its halo-model representation.

The absence of clear information on the 3D displacement of the physical results as a function of the redshift and the selected magnitude characterize the cosmological N-body, the dynamical and the hydrodynamical models. This absence of detailed information leads to the analysis of the following questions:

- Is it possible to compare the theoretical and observational number of galaxies as a function of the redshift for a fixed flux/magnitude ?
- What is the role of the Malmquist bias when theoretical and observed numbers of galaxies versus the redshift are compared?
- Is it possible to find an algorithm which describes the intersection between a slice that starts from the center of the box and the faces of irregular Poissonian Voronoi Polyhedrons?
- Is it possible to model the intersection between a sphere of a given redshift and the faces of irregular Poissonian Voronoi Polyhedrons?
- Does the developed theory match the observed slices of galaxies as given, for example, by the 2dF Galaxy Redshift Survey?
- Does the developed algorithm explain the voids appearance in all sky surveys such as the RC3?
- Can voids between galaxies be modeled through the Voronoi normalized volume distribution?
- Is it possible to evaluate the probability of having a supervoid once the averaged void's diameter is fixed?
- Is it possible to compute the correlation function for galaxies by introducing the concept of thick faces of irregular Voronoi polyhedrons?
- Is it possible to find the acoustic oscillations of the correlation function at $\approx 100Mpc$ in simulated slices of the Voronoi diagrams.

In order to answer these questions, Section 2 briefly reviews the standard luminosity function for galaxies. An accurate test of the number of galaxies as a function of the redshift is performed on the 2dF Galaxy Redshift Survey (2dFGRS), see Section 3. Section 4 reports the technique which allows us to extract the galaxies belonging to the Voronoi polyhedron and Section 5 simulates the redshift dependence of the 2dFGRS as well as the overall Third Reference Catalog of Bright Galaxies (RC3). Section 6 reports the simulation of the correlation function computed on the thick faces of the Voronoi polyhedron.

2 Useful formulas

Starting from Hubble (1929) the suggested correlation between expansion velocity and distance is

$$V = H_0 D = c_l z \quad , \quad (1)$$

where the Hubble constant is $H_0 = 100h \text{ km s}^{-1} \text{ Mpc}^{-1}$, with $h = 1$ when h is not specified, D is the distance in Mpc , c_l is the light velocity and z is the redshift. Concerning the value of H_0 we will adopt a recent value as obtained by the Cepheid-calibrated luminosity of Type Ia supernovae, see Sandage et al. (2006),

$$H_0 = (62.3 \pm 5) \text{ km s}^{-1} \text{ Mpc}^{-1} \quad . \quad (2)$$

The quantity $c_l z$, a velocity, or z , a number, characterizes the catalog of galaxies.

We recall that the galaxies have peculiar velocities, making the measured redshifts a combination of cosmological redshift plus a contribution on behalf of the peculiar velocity.

The maximum redshift here considered is $z \approx 0.1$ meaning a maximum velocity of expansion of $\approx 30000 \frac{Km}{s}$; up to that value the space is assumed to be Euclidean. We now report the joint distribution in z and f (the flux of radiation) for galaxies adopting the Schechter function for the luminosity (L) of galaxies, $\Phi(L)$, introduced by Schechter (1976) and the mass-luminosity relationship, $\Psi(L)$, as derived in Zaninetti (2008). The joint distribution in z and f for the Schechter function, see formula (1.104) in Padmanabhan (1996) or formula (1.117) in Padmanabhan (2002) , is

$$\frac{dN}{d\Omega dz df} = 4\pi \left(\frac{c_l}{H_0}\right)^5 z^4 \Phi\left(\frac{z^2}{z_{crit}^2}\right) \quad , \quad (3)$$

where $d\Omega$, dz and df represent the differential of the solid angle , the redshift and the flux respectively. The critical value of z , z_{crit} , is

$$z_{crit}^2 = \frac{H_0^2 L^*}{4\pi f c_l^2} \quad . \quad (4)$$

The number of galaxies, $N_S(z, f_{min}, f_{max})$ comprised between a minimum value of flux, f_{min} , and maximum value of flux f_{max} , can be computed

through the following integral

$$N_S(z) = \int_{f_{min}}^{f_{max}} 4\pi \left(\frac{c_l}{H_0}\right)^5 z^4 \Phi\left(\frac{z^2}{z_{crit}^2}\right) df \quad . \quad (5)$$

This integral does not have an analytical solution and therefore a numerical integration must be performed.

The number of galaxies in z and f as given by formula (3) has a maximum at $z = z_{pos-max}$, where

$$z_{pos-max} = z_{crit} \sqrt{\alpha + 2} \quad , \quad (6)$$

where α sets the slope for low values of L . This position can be re-expressed as

$$z_{pos-max} = \frac{\sqrt{2 + \alpha} \sqrt{10^{0.4 M_{\odot} - 0.4 M^*}} H_0}{2 \sqrt{\pi} \sqrt{f} c_l} \quad , \quad (7)$$

where M_{\odot} is the reference magnitude of the sun at the considered band-pass and M^* is the characteristic magnitude as derived from the data. The joint distribution in z and f , in presence of the $\mathcal{M} - L$ relationship, see equation (38) Zaninetti (2008), is

$$\frac{dN}{d\Omega dz df} = 4\pi \left(\frac{c_l}{H_0}\right)^5 z^4 \Psi\left(\frac{z^2}{z_{crit}^2}\right) \quad . \quad (8)$$

The number of galaxies, $N_{\mathcal{M}-L}(z, f_{min}, f_{max})$ with flux comprised between f_{min} and f_{max} , can be computed through the following integral

$$N_{\mathcal{M}-L}(z) = \int_{f_{min}}^{f_{max}} 4\pi \left(\frac{c_l}{H_0}\right)^5 z^4 \Psi\left(\frac{z^2}{z_{crit}^2}\right) df \quad , \quad (9)$$

and also in this case a numerical integration must be performed.

The number of galaxies as given by the $\mathcal{M} - L$ relationship has a maximum at $z_{pos-max}$, see equation (41) in Zaninetti (2008)

$$z_{pos-max} = z_{crit} (c + a)^{a/2} \quad , \quad (10)$$

which can be re-expressed as

$$z_{pos-max} = \frac{(a + c)^{1/2 a} \sqrt{10^{0.4 M_{\odot} - 0.4 M^*}} H_0}{2 \sqrt{\pi} \sqrt{f} c_l} \quad , \quad (11)$$

where $1/a$ is an exponent which connects mass to luminosity and c represents the dimensionality of the fragmentation.

Table 1: The parameters of the Schechter function for the 2dFGRS as in Madgwick et al. 2002.

<i>parameter</i>	<i>2dFGRS</i>
$M^* - 5 \log_{10} h$ [mags]	(-19.79 ± 0.04)
α	-1.19 ± 0.01
Φ^* [$h^3 \text{ Mpc}^{-3}$]	$((1.59 \pm 0.1)10^{-2})$

Table 2: The parameters of the $\mathcal{M} - L$ luminosity function based on the 2dFGRS data (triplets generated by the author).

	<i>2dFGRS</i>
c	0.1
$M^* - 5 \log_{10} h$ [mags]	-19 ± 0.1
Ψ^* [$h^3 \text{ Mpc}^{-3}$]	0.4 ± 0.01
a	1.3 ± 0.1

3 Photometric test on the catalog

We now check the previously derived formulas on a catalog of galaxies. A first example is the 2dFGRS data release available on the web site: <http://msowww.anu.edu.au/2dFGRS>. In particular we added together the file parent.ngp.txt which contains 145652 entries for NGP strip sources and the file parent.sgp.txt which contains 204490 entries for SGP strip sources. Once the heliocentric redshift was selected we processed 219107 galaxies with $0.001 \leq z \leq 0.3$. The parameters of the Schechter function concerning the 2dFGRS can be found in the first line of Table 3 in Madgwick et al. (2002) and are reported in Table 1. It is interesting to point out that other values for h different from 1 shift all absolute magnitudes by $5 \log_{10} h$ and change number densities by the factor h^3 .

Before reducing the data we should discuss the Malmquist bias, see Malmquist

(1920, 1922), that was originally applied to the stars and was then applied to the galaxies by Behr (1951). We therefore introduce the concept of limiting apparent magnitude and the correspondent completeness in absolute magnitude of the considered catalog as a function of the redshift. The observable absolute magnitude as a function of the limiting apparent magnitude, m_L , is

$$M_L = m_L - 5 \log_{10} \left(\frac{c_L z}{H_0} \right) - 25 \quad . \quad (12)$$

The previous formula predicts, from a theoretical point of view the upper limit of the absolute maximum magnitude that can be observed in a catalog of galaxies characterized by a given limiting magnitude. The interval covered by the LF for galaxies, ΔM , is defined as

$$\Delta M = M_{max} - M_{min} \quad , \quad (13)$$

where M_{max} and M_{min} are the maximum and minimum absolute magnitude of the LF for the considered catalog. The real observable interval in absolute magnitude, ΔM_L , is

$$\Delta M_L = M_L - M_{min} \quad . \quad (14)$$

We can therefore introduce the range of observable absolute maximum magnitude expressed in percent, $\epsilon(z)$, as

$$\epsilon_s(z) = \frac{\Delta M_L}{\Delta M} \times 100 \quad . \quad (15)$$

This is a number that represents the completeness of the sample and given the fact that the limiting magnitude of the 2dFGRS is $m_L=19.61$ it is possible to conclude that the 2dFGRS is complete for $z \leq 0.0442$. Figure 1 and Figure 2 report the number of observed galaxies of the 2dFGRS catalog for two different apparent magnitudes and two theoretical curves as represented by formula (3) and formula (8).

Due to the importance of the maximum as a function of z in the number of galaxies, Figure 3 reports the observed histograms in the 2dFGRS and the theoretical curves as a function of the magnitude.

Following is an outline of the sources of discrepancy between theory (equations (3) and (8))

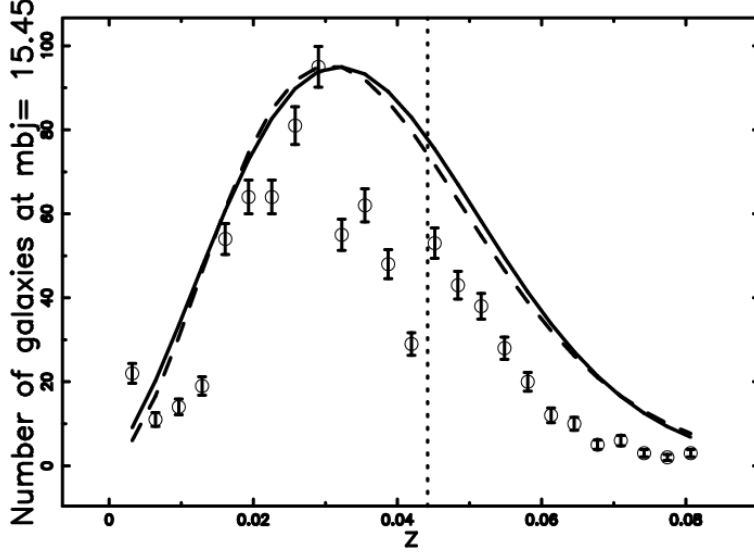


Figure 1: The galaxies of the 2dFGRS with $15.27 \leq bJmag \leq 15.65$ or $59253 \frac{L_{\odot}}{Mpc^2} \leq f \leq 83868 \frac{L_{\odot}}{Mpc^2}$ (with $bJmag$ representing the relative magnitude used in object selection), are isolated in order to represent a chosen value of m and then organized in frequencies versus heliocentric redshift, (empty circles); the error bar is given by the square root of the frequency. The maximum in the frequencies of observed galaxies is at $z = 0.03$. The maximum of the observed galaxies can also be computed through the maximum likelihood estimator (MLE) by adopting the Schechter function for the luminosity, see Appendix A; $\hat{z}_{pos-max} = 0.033$ according to equation (A.6). The theoretical curve generated by the Schechter function of luminosity (formula (3) and parameters as in column 2dFGRS of Table 1) is drawn (full line). The theoretical curve generated by the $\mathcal{M} - L$ function for luminosity (formula (8) and parameters as in column 2dFGRS of Table 2) is drawn (dashed line); $\chi^2 = 550$ for the Schechter function and $\chi^2 = 503$ for the $\mathcal{M} - L$ function. In this plot $\mathcal{M}_{\odot} = 5.33$ and $h = 0.623$. The vertical dotted line represents the boundary between complete and incomplete samples.

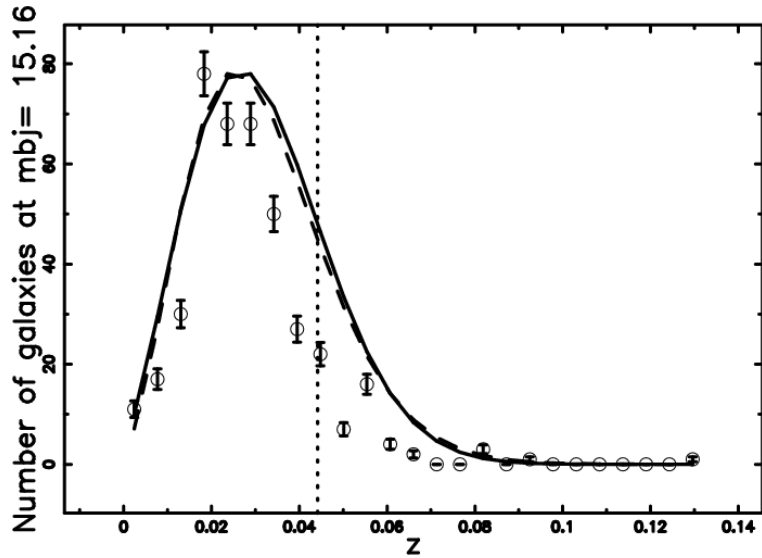


Figure 2: The galaxies in the 2dFGRS with $15.02 \leq bJmag \leq 15.31$ or $80527 \frac{L_{\odot}}{Mpc^2} \leq f \leq 105142 \frac{L_{\odot}}{Mpc^2}$. The maximum in the frequencies of observed galaxies is at $z = 0.02$, $\chi^2 = 256$ for the Schechter function (full line) and $\chi^2 = 224$ for the $\mathcal{M} - L$ function (dashed line). The maximum of the observed galaxies can also be computed through the maximum likelihood estimator (MLE) by adopting the the Schechter function for the luminosity, see Appendix A; $\hat{z}_{pos-max} = 0.031$ according to equation (A.6). In this plot $\mathcal{M}_{\odot} = 5.33$ and $h = 0.623$. The vertical dotted line represents the boundary between complete and incomplete samples.

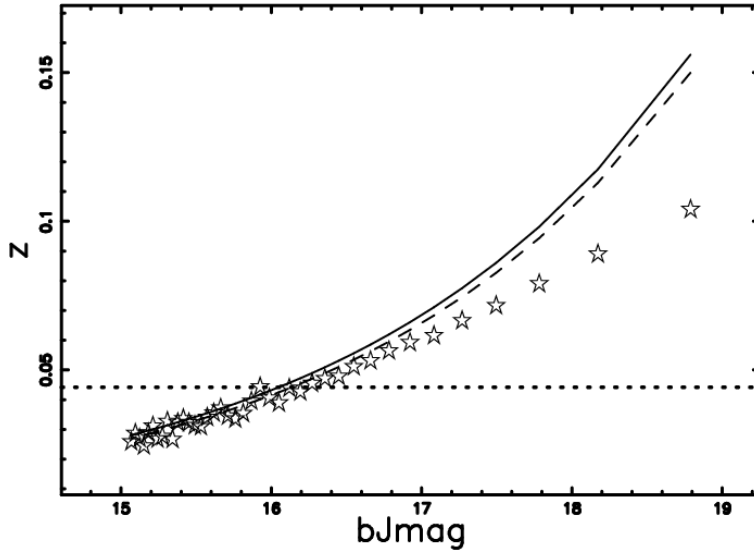


Figure 3: Value of $\hat{z}_{pos-max}$ (see equation A.6) at which the number of galaxies in the 2dFGRS is maximum as a function of the apparent magnitude $bJmag$ (stars), theoretical curve of the maximum for the Schechter function as represented by formula (7) (full line) and theoretical curve of the maximum for the $\mathcal{M} - L$ function as represented by formula (11) (dashed line). In this plot $\mathcal{M}_{\odot} = 5.33$ and $h=0.623$. The horizontal dotted line represents the boundary between complete and incomplete samples.

- The density of galaxies is assumed to be constant in deriving the theoretical equations. In a cellular structure of the universe with the galaxies situated on the faces of irregular polyhedrons, the number of galaxies varies with r^2 , where r is the progressive distance from the center of the box, up to a distance equal to the averaged diameter of a polyhedron. After that distance the number of galaxies grows as r^3 .
- The interval in magnitude should be chosen in order to be smaller than the error in magnitude.
- A limited range in z should be considered in order to satisfy the Malmquist bias.

The total number of galaxies in the 2dFGRS is reported in Figure 4 as well as the theoretical curves as represented by the numerical integration of formula (3) and formula (8). In this section we have adopted the absolute magnitude of the sun in the b_j filter $\mathcal{M}_{\odot} = 5.33$, see Tempel et al. (2009); Eke et al. (2004).

4 The 3D Voronoi Diagrams

The observational fact that the galaxies seem to be distributed on almost bubble like surfaces, surrounding large empty regions allows us to introduce the geometrical properties of irregular Voronoi Polyhedron as a useful tool to explain the galaxy's network. The faces of the Voronoi Polyhedra share the same property, i.e. they are equally distant from two nuclei. The intersection between a plane and the faces produces diagrams which are similar to the edges' displacement in 2D Voronoi diagrams. From the point of view of the observations it is very useful to study the intersection between a slice which crosses the center of the box and the faces of irregular polyhedrons where presumably the galaxies reside. The general definition of the 3D Voronoi Diagrams is given in Section 4.1. The intersection between a slice of a given opening angle, for example 3° , and the faces of the Voronoi Polyhedra can be realized through an approximate algorithm, see next Section 4.2. The volumes of the Voronoi Polyhedra can be identified by the voids between galaxies, while the statistics that describe the volumes can help to study the statistics of the void's size distribution in the 2dFGRS, see von Benda-Beckmann & Müller (2008).

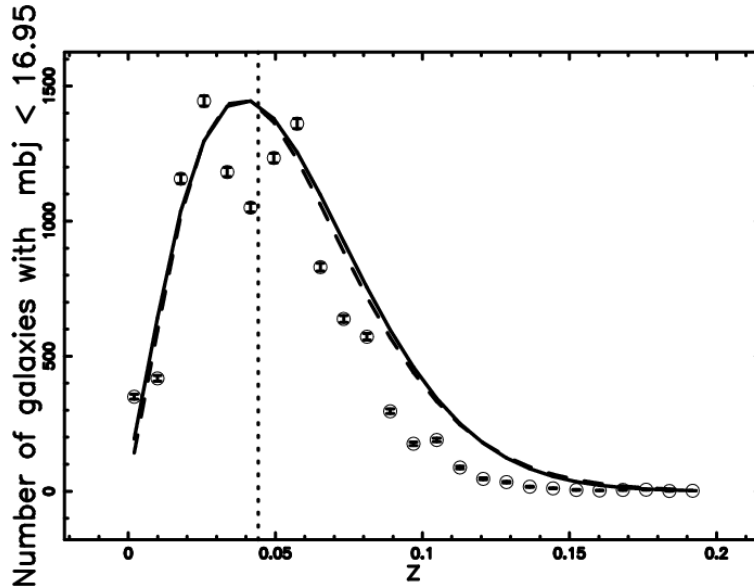


Figure 4: The galaxies in the 2dFGRS with $13.34 \leq bJmag \leq 16.94$ or $17950 \frac{L_{\odot}}{Mpc^2} \leq f \leq 493844 \frac{L_{\odot}}{Mpc^2}$, are organized in frequencies versus heliocentric redshift, (empty stars). The theoretical curves generated by the integral of the Schechter function in flux (formula (5) with parameters as in Table 1) (full line) and by the integral of the $\mathcal{M} - L$ function as represented by formula (9) with parameters as in column 2dFGRS of Table 2) (dashed line) are drawn. The maximum in the frequencies of observed galaxies is at $z = 0.029$, $\chi^2 = 3314$ for the Schechter function (full line) and $\chi^2 = 3506$ for the $\mathcal{M} - L$ function (dashed line). In this plot $\mathcal{M}_{\odot} = 5.33$ and $h = 0.623$. The vertical dotted line represents the boundary between complete and incomplete sample.

4.1 General Definition

The Voronoi diagram for a set of seeds, S , located at position x_i in \mathcal{R}^3 space is the partitioning of that space into regions such that all locations within any one region are closer to the generating point than to any other. The points closer to one seed than another are divided by the perpendicular bisecting plane between the two seeds. For a random tessellation, only a finite number of half-planes bind the cell, so the cell is a convex polyhedron. It follows that a plane cross-section of a 3D tessellation is a tessellation of the plane composed of convex polygons. The points of a 3D tessellation are of four types, depending on how many nearest neighbors in S they have. A point with exactly one nearest neighbor is in the interior of a cell, a point with two nearest neighbors is on the face between two cells, a point with three nearest neighbors is on an edge shared by three cells, and a point with four neighbors is a vertex where three cells meet. There is zero probability that there will be any point with five or more nearest neighbors. In the following we will work on a three dimensional lattice defined by $pixels \times pixels \times pixels$ points, L_{kmn} .

The Voronoi polyhedron V_i around a given center i , is the set of lattice points L_{kmn} closer to i than to any j : more formally,

$$L_{kmn} \in V_i \leftrightarrow |x_{kmn} - x_i| \leq |x_{kmn} - x_j|, \quad (16)$$

where x_{kmn} denotes the lattice point position. Thus, the Polyhedra are intersections of half-spaces. Given a center i and its neighbor j , the line ij is cut perpendicularly at its midpoint y_{ij} by the plane h_{ij} . H_{ij} is the half-space generated by the plane h_{ij} , which consists of the subset of lattice points on the same side of h_{ij} as i ; therefore

$$V_i = \cap_j H_{ij}, \quad (17)$$

V_i is bounded by faces, with each face f_{ij} belonging to a distinct plane h_{ij} . Each face will be characterized by its vertices and edges.

4.2 The adopted algorithm

Our method considers a 3D lattice with $pixels^3$ points: present in this lattice are N_s seeds generated according to a random process. All the computations

are usually performed on this mathematical lattice; the conversion to the physical lattice is obtained by multiplying the unit by $\delta = \frac{side}{pixels-1}$, where *side* is the length of the cube expressed in the physical unit adopted. In order to minimize boundary effects introduced by those polyhedron which cross the cubic boundary, the cube in which the seeds are inserted is amplified by a factor *amplify*. Therefore the N_s seeds are inserted in a volume $pixels^3 \times amplify$, which is bigger than the box over which the scanning is performed; *amplify* is generally taken to be equal to 1.2. This procedure inserts periodic boundary conditions to our cube. A sensible and solid discussion of what such an extension of a cube should be can be found in Neyrinck et al. (2005). The set S of the seeds can be of Poissonian or non-Poissonian type. Adopting the point of view that the universe should be the same from each point of view of the observer the Poissonian seeds can represent the best choice in order to reproduce the large scale structures.

The Poissonian seeds are generated independently on the X , Y and Z axis in 3D through a subroutine which returns a pseudo-random real number taken from a uniform distribution between 0 and 1. For practical purposes, the subroutine RAN2 was used, see Press et al. (1992). Particular attention should be paid to the average observed diameter of voids, \overline{DV}^{obs} , here chosen as

$$\overline{DV}^{obs} \approx 0.6 DV_{max}^{obs} = 2700 \frac{Km}{sec} \quad , \quad (18)$$

where $DV_{max}^{obs} = 4500 \frac{Km}{sec}$ corresponds to the extension of the maximum void visible, for example, on the CFA2 slices, see Geller & Huchra (1989). The corresponding diameter, \overline{DV}^{obs} , in *pc* is

$$\overline{DV}^{obs} = \frac{27}{h} Mpc \quad . \quad (19)$$

The number of Poissonian seeds is chosen in such a way that the averaged volume occupied by a Voronoi polyhedron is equal to the averaged observed volume of the voids in the spatial distribution of galaxies; more details can be found in Zaninetti (2006). It is possible to plot the cumulative volume-weighted void size distribution, $F(> R)$, in the 2dFGRS samples, see Figure 4 in von Benda-Beckmann & Müller (2008). From the previous figure it is possible to make a graphical evaluation of the value of R at which $F(> R) = 1/2$, the median of the probability density function connected with $F(> R)$. The median value of R from Figure 4 in von Benda-Beckmann & Müller

(2008) turns out to be $5 \text{ Mpc} < R < 12 \text{ Mpc}$ according to the four models there implemented. The average value of R here assumed to be $\frac{13.5}{h} \text{ Mpc}$ is not far from the median value presented in von Benda-Beckmann & Müller (2008).

We now work on a 3D lattice $L_{k,m,n}$ of *pixels*³ elements. Given a section of the cube (characterized, for example, by $k = \frac{\text{pixels}}{2}$) the various V_i (the volume belonging to the seed i) may or may not cross the pixels belonging to the two dimensional lattice. A typical example of a 2D cut organized in two strips about 75° long is visible in Figure 5 where the Cartesian coordinates X and Y with the origin of the axis at the center of the box has been used. The previous cut has an extension on the Z -axis equal to zero.

Conversely Figure 6 reports two slices of 75° long and 3° wide. In this case the extension of the enclosed region belonging to the Z -axis increases with distance according to

$$\Delta Z = \sqrt{X^2 + y^2} \tan \frac{\alpha}{2} \quad , \quad (20)$$

where ΔZ is the thickness of the slice and α is the opening angle, in our case 3° .

In order to simulate the slices of observed galaxies a subset is extracted (randomly chosen) of the pixels belonging to a slice as represented, for example, in Figure 6. In this operation of extraction of the galaxies from the pixels of the slice, the photometric rules as represented by formula (3) must be respected.

The cross sectional area of the VP can also be visualized through a spherical cut characterized by a constant value of the distance to the center of the box, in this case expressed in z units, see Figure 7 and Figure 8; this intersection is called $V_s(2,3)$ where the index s stands for sphere.

4.3 The statistics of the volumes

The distribution of volumes in the Poissonian Voronoi Diagrams can be modeled by the following probability density function (PDF) $H(x; c_k)$

$$H(x; c_k) = \frac{c_k}{\Gamma(c_k)} (c_k x)^{c_k-1} \exp(-c_k x) \quad , \quad (21)$$

where $0 \leq x < \infty$, $c_k > 0$ and $\Gamma(c_k)$ is the gamma function with argument c_k , see formula (5) by Kiang (1966) . According to the "Kiang conjecture"

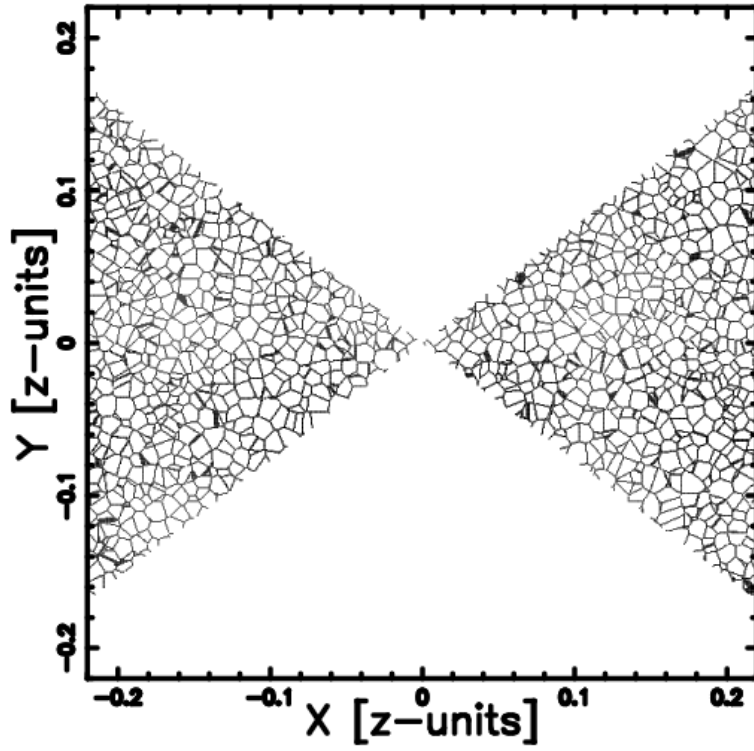


Figure 5: Portion of the Poissonian Voronoi-diagram $V_p(2,3)$; cut on the X-Y plane when two strips of 75° are considered. The parameters are $pixels=600$, $N_s = 137998$, $side = 131908 \text{ Km/sec}$ and $amplify = 1.2$.

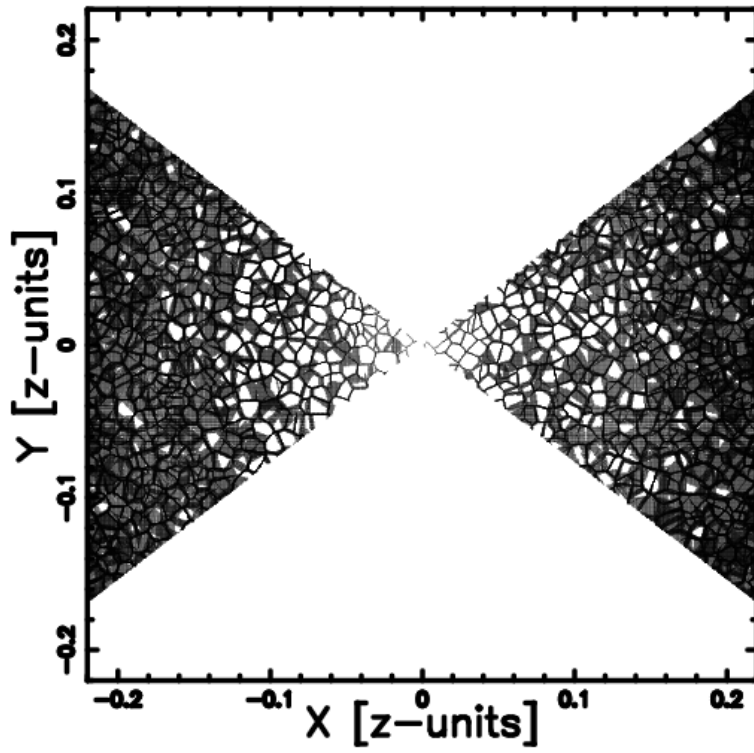


Figure 6: The same as Figure 5 but now two slices of 75° long and 3° wide are considered.

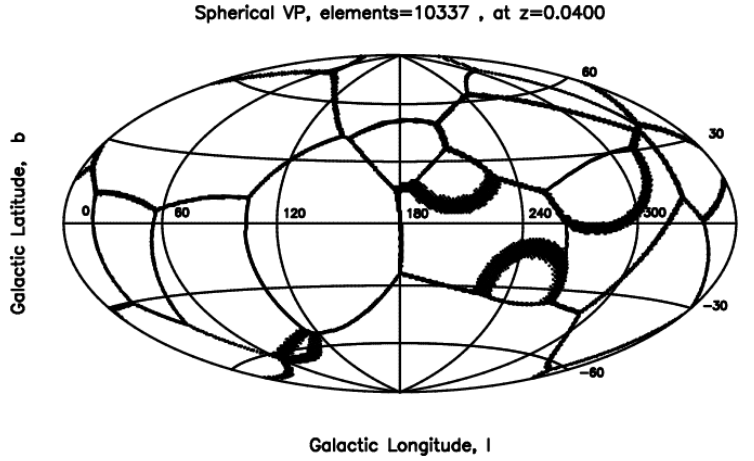


Figure 7: The Voronoi-diagram $V_s(2, 3)$ in the Hammer-Aitoff projection at $z = 0.04$. The parameters are $pixels = 400$, $N_s = 137998$, $side = 131908$ Km/sec and $amplify = 1.2$.

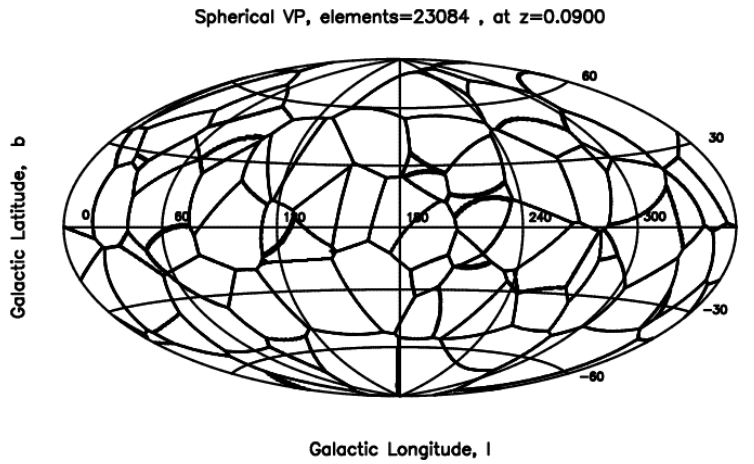


Figure 8: The Voronoi-diagram $V_s(2, 3)$ in the Hammer-Aitoff projection at $z = 0.09$; other parameters as in Figure 7.

Table 3: The χ^2 of data fit when the number of classes is 40 for three PDF

<i>PDF</i>	χ^2
$H(x; d)$ when $d = 3$ ($c_k = 6$)	1778
$H(x; d)$ when $d = 2.75$ ($c_k = 5.5$)	414
$FN(x; d)$ Ferenc & Neda formula (23) when $d = 3$	565

the volumes should be characterized by $c_k = 6$, see Zaninetti (2008) for more details. This PDF can be generalized by introducing the dimension of the considered space, d ($d = 1, 2, 3$), and $c_k = 2d$

$$H(x; d) = \frac{2d}{\Gamma(2d)} (2dx)^{2d-1} \exp(-2dx) \quad . \quad (22)$$

A new analytical PDF is

$$FN(x; d) = Const \times x^{\frac{3d-1}{2}} \exp(-(3d+1)x/2) \quad , \quad (23)$$

where

$$Const = \frac{\sqrt{2}\sqrt{3d+1}}{2 \cdot 2^{3/2d} (3d+1)^{-3/2d} \Gamma(3/2d + 1/2)} \quad , \quad (24)$$

and d ($d = 1, 2, 3$) represents the dimension of the considered space, see Ferenc & Neda (2007). In the two PDF here presented, equation (23) and equation (22), the statistics of the volumes are obtained by inserting $d = 3$. In order to obtain the volumes in every point-lattice $L_{k,m,n}$ we computed the nearest seed and increased by one the volume of that seed. The frequency histogram and the relative best fit through gamma-variate PDF for the volume distribution is reported in Figure 9; Figure 10 conversely reports the fit with PDF (23) by Ferenc & Neda (2007).

The results are reported in Table 3 and it is possible to conclude that the volume distribution of irregular Voronoi polyhedron is better described by PDF (23) in Ferenc & Neda (2007) rather than the sum of three gamma variates with argument 2. When conversely d is used as a free parameter to be deduced from the sample in PDF (22) we obtain a smaller χ^2 with respect to the function in Ferenc & Neda (2007).

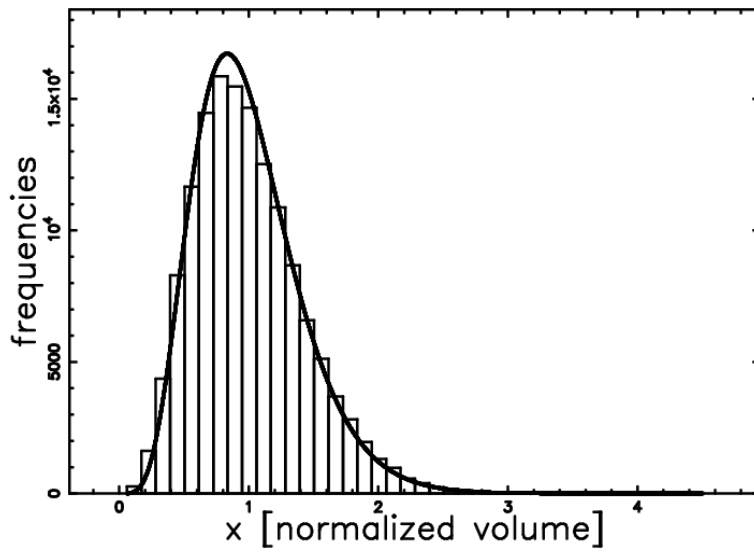


Figure 9: Histogram (step-diagram) of the Voronoi normalized volume distribution in 3D with a superposition of the gamma-variate as represented by equation (22). Parameters as in Figure 5 but $pixels = 500$: $d=3$, $NBIN=40$ and $\chi^2=1778$

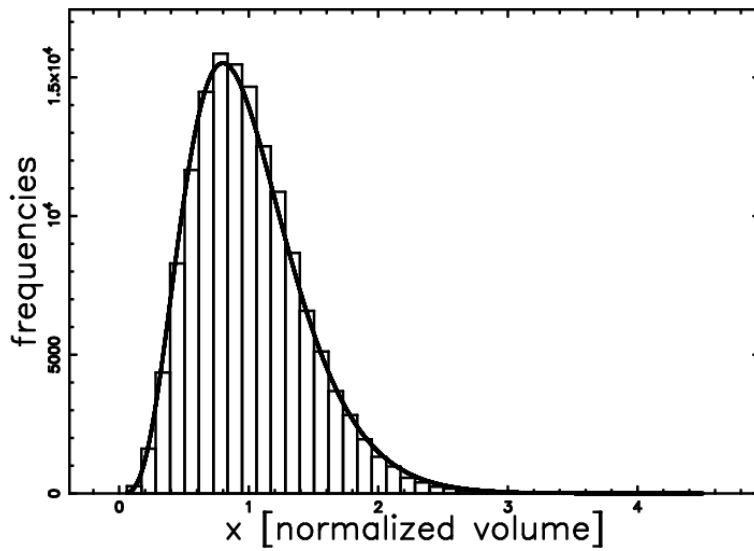


Figure 10: Histogram (step-diagram) of the Voronoi normalized volume distribution in 3D with a superposition of the gamma PDF as represented by equation (23) first introduced in Ferenc & Neda 2007. Parameters as in Figure 5 but $pixels = 500$: $d=3$, $NBIN=40$ and $\chi^2=565$

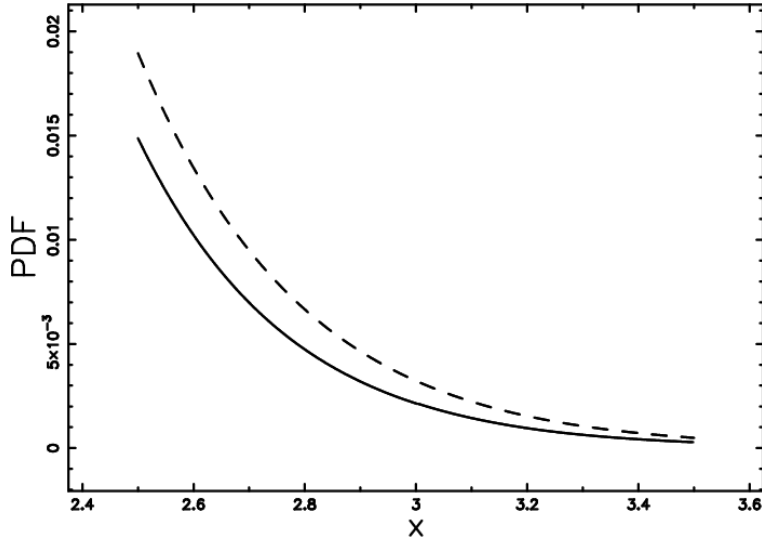


Figure 11: Plot of Voronoi normalized volume-distribution in 3D when 2 PDFs are adopted: $k(x;d)$ (Eq. (22)), $d=2.75$ (full line) and $FN(x;d)$ (Eq.(23)), $d=3$, (dashed).

On summarizing the differences between the Kiang function and the Ferenc & Neda function we can say that the Kiang function (equation(22)) requires the numerical evaluation of the free parameter $d = c_k/2$. In the case of Ferenc & Neda (equation (23)) the number of free parameters is zero once $d = 3$ is inserted. The numerical difference between the two PDFs is reported in Figure 11 for large values of the normalized volume distribution.

5 The cellular structure of the Universe

From a simplified point of view the galaxies belonging to a given catalog are characterized by the astronomical coordinates, the redshift and the apparent magnitude. Starting from the second CFA2 redshift Survey, the catalogs were organized in slices of a given opening angle, 3° or 6° , and a given angular extension, for example 130° . When plotted in polar coordinates of $c_l z$ the spatial distribution of galaxies is not random but distributed on filaments.

Particular attention should be paid to the fact that the astronomical slices are not a plane which intersects a Voronoi Network. In order to quantify this effect we introduce a confusion distance, DV_c , as the distance after which the half altitude of the slices equalizes the observed average diameter \overline{DV}^{obs}

$$DV_c \tan(\alpha) = \frac{1}{2} \overline{DV}^{obs} \quad , \quad (25)$$

where α is the opening angle of the slice and \overline{DV}^{obs} the averaged diameter of voids. In the case of 2dFGRS $\alpha = 3^\circ$ and therefore $DV_c = 2.57 \cdot 10^4 \frac{Km}{sec}$ when $\overline{DV}^{obs} = 2700 \frac{Km}{sec}$. For values of $c_l z$ greater than DV_c the voids in the distribution of galaxies are dominated by the confusion. For values of $c_l z$ lower than DV_c the filaments of galaxies can be considered the intersection between a plane and the faces of the Voronoi Polyhedrons. A measure of the portion of the sky covered by a catalog of galaxies is the area covered by a unitarian sphere which is 4π steradians or $\frac{129600}{\pi}$ square degrees. In the case of 2dFGRS the covered area of two slices of 75° long and 3° wide, as in Figure 14, is $\frac{1414}{\pi}$ square degrees or 0.13 sr . In the case of RC3 the covered area it is 4π steradians with the exclusion of the *Zone of Avoidance*, see Figure 17. In the following we will simulate the 2dFGRS, a catalog that occupies a small area of the sky and RC3, a catalog that occupies all the sky.

In the case of 3C3 we demonstrate how it is possible to simulate the *Zone of Avoidance* in the theoretical simulation. The paragraph ends with a discussion on the Eridanus supervoid also known as "Cold Spot".

5.1 The 2dFGRS

The survey consists of two separate declination strips: one strip (the SGP strip) is in the southern Galactic hemisphere and covers approximately $80^\circ \times 15^\circ$ centered close to the South Galactic Pole. The second strip (the NGP strip) is in the northern Galactic hemisphere and covers $80^\circ \times 15^\circ$, see Colless et al. (2001).

Figure 12 shows the galaxies of the 2dFGRS with $z < 0.3$ in galactic coordinates and the two strips in the 2dFGRS are shown in Figure 13.

Figure 14 conversely reports the 2dFGRS catalog when a slice of $75^\circ \times 3^\circ$ is taken into account. This slice represents the object to simulate.

The previous observational slice can be simulated by adopting the Voronoi network reported in Figure 6.

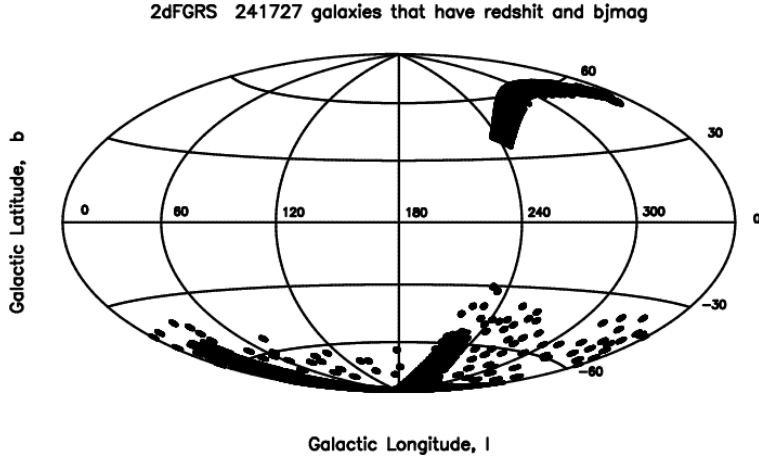


Figure 12: Hammer-Aitoff projection in galactic coordinates of 230540 galaxies in the 2dfGRS which have bJmag and redshift < 0.3 .

The distribution of the galaxies as given by the Voronoi Diagrams is reported in Figure 15 where all the galaxies are considered. In this case the galaxies are extracted according to the integral of the Schechter function in flux (formula (5) with parameters as in Table 1). Table 4 reports the basic data of the astronomical and simulated data of the $75^\circ \times 3^\circ$ slice.

When conversely a given interval in flux (magnitudes) characterized by f_{min} and f_{max} is considered the number of galaxies, N_{SC} , of a 3° slice can be found with the following formula

$$N_{SC} = N_C \frac{\int_{f_{min}}^{f_{max}} 4\pi \left(\frac{c_l}{H_0}\right)^5 z^4 \Phi\left(\frac{z^2}{z_{crit}^2}\right) df}{\int_{f_{min,C}}^{f_{max,C}} 4\pi \left(\frac{c_l}{H_0}\right)^5 z^4 \Phi\left(\frac{z^2}{z_{crit}^2}\right) df} , \quad (26)$$

where $f_{min,C}$ and $f_{max,C}$ represent the minimum and maximum flux of the considered catalog and N_C all the galaxies of the considered catalog; a typical example is reported in Figure 16.

5.2 The Third Reference Catalog of Bright Galaxies

The RC3, see de Vaucouleurs et al. (1991), is available at the following address <http://vizier.u-strasbg.fr/viz-bin/VizieR?-source=VII/155>.

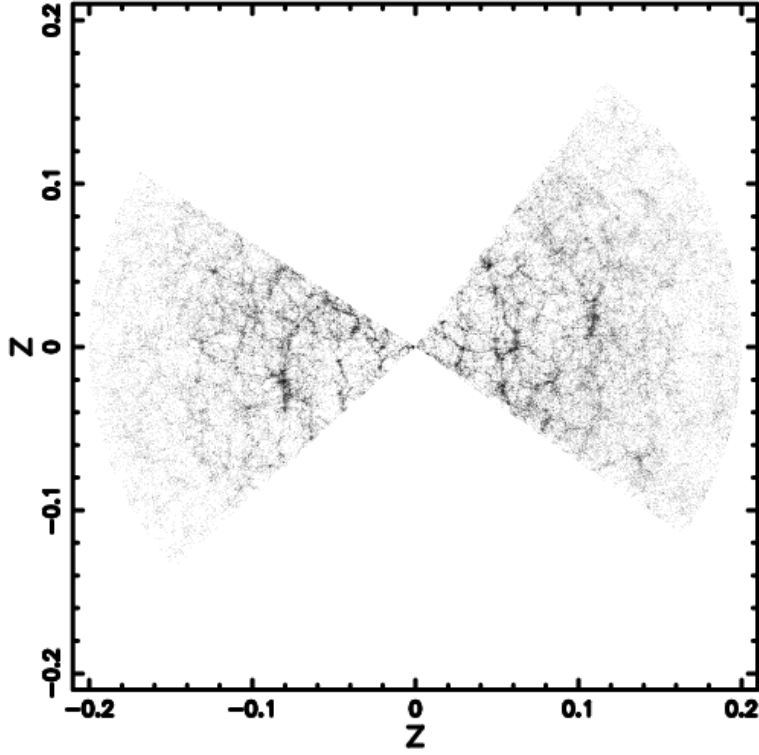


Figure 13: Cone-diagram of all the galaxies in the 2dFGRS. This plot contains 203249 galaxies.

Table 4: Real and Simulated data of the slice 75° long and 3° .

	<i>2dFGRS</i>	<i>simulation</i>
<i>elements</i>	62559	62563
z_{min}	0.001	0.011
$z_{pos-max}$	0.029	0.042
z_{ave}	0.051	0.058
z_{max}	0.2	0.2

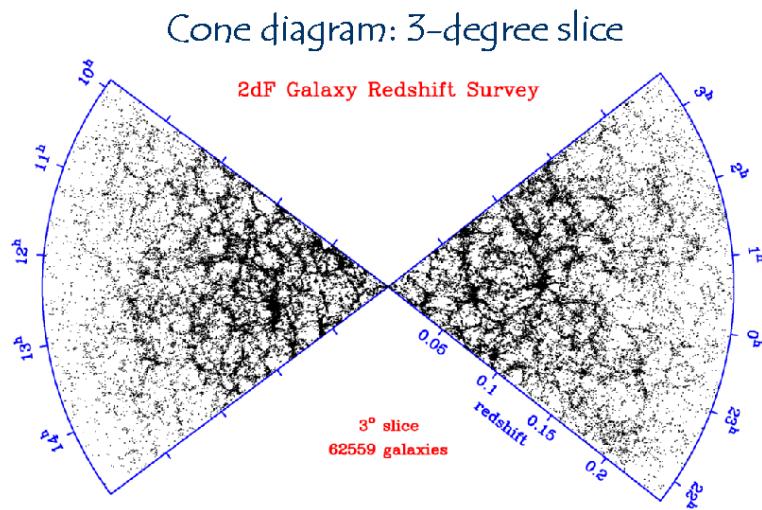


Figure 14: Slice of $75^\circ \times 3^\circ$ in the 2dFGRS. This plot contains 62559 galaxies and belongs to the 2dFGRS Image Gallery available at the web site: <http://msowww.anu.edu.au/2dFGRS/>.

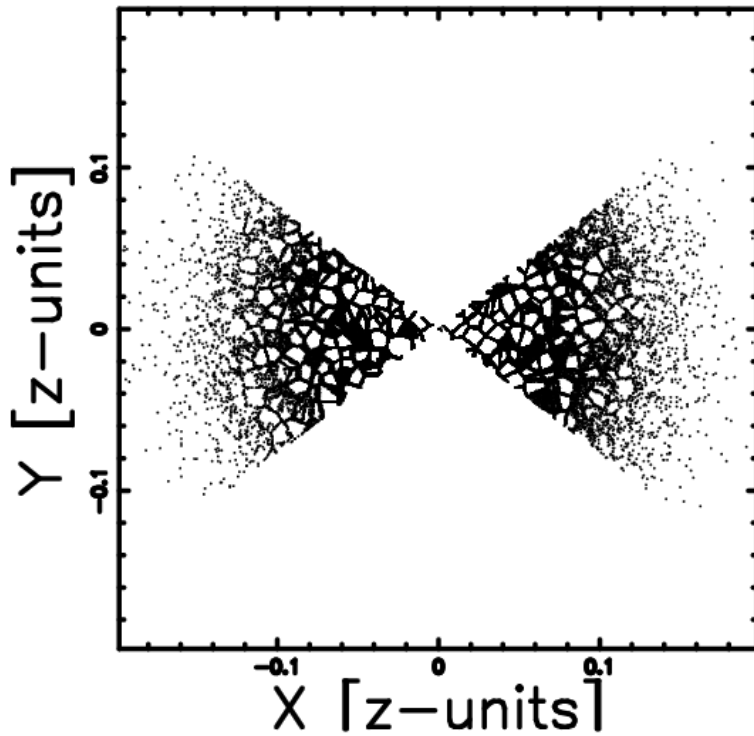


Figure 15: Polar plot of the pixels belonging to a slice 75° long and 3° wide. This plot contains 62563 galaxies, the maximum in the frequencies of theoretical galaxies is at $z = 0.043$. In this plot $\mathcal{M}_\odot = 5.33$ and $h=0.623$.

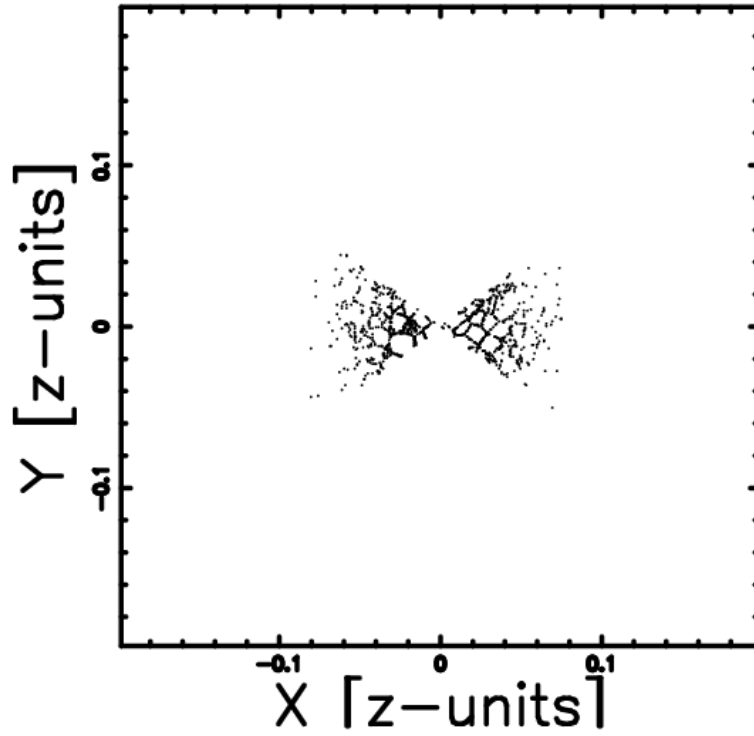


Figure 16: Polar plot of the pixels belonging to a slice 75° long and 3° wide. Galaxies with magnitude $15.02 \leq bJmag \leq 15.31$ or $46767 \frac{L_\odot}{Mpc^2} \leq 61063 \frac{L_\odot}{Mpc^2}$. The maximum in the frequencies of theoretical galaxies is at $z = 0.029$, $N_{SC}=2186$ and $N_C=62559$. In this plot $\mathcal{M}_\odot = 5.33$ and $h=0.623$.

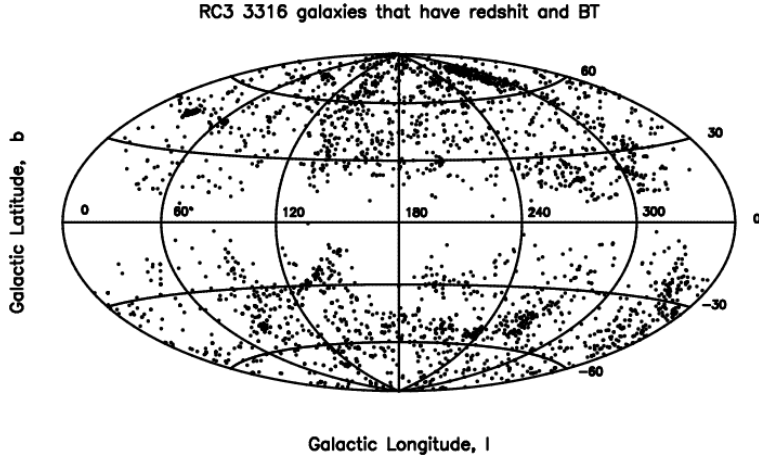


Figure 17: Hammer-Aitoff projection in galactic coordinates of 3316 galaxies in the RC3 which have BT and redshift.

This catalog attempts to be reasonably complete for galaxies having apparent diameters larger than 1 arcmin at the D25 isophotal level and total B-band magnitudes BT, brighter than about 15.5, with a redshift not in excess of 15000 km/s. All the galaxies in the RC3 catalog which have redshift and BT are reported in Figure 17. Figure 18 reports the RC3 galaxies in a given window in z . We now test the concept of an isotropic universe. This can be done by plotting the number of galaxies comprised in a slice of 360° in galactic longitude versus a variable number Δb in galactic latitude, for example 6° . The number of galaxies in the RC3 versus galactic latitude is plotted in Figure 19.

The solid angle $d\Omega$ in spherical coordinates (r, θ, ϕ) is

$$d\Omega = \sin(\theta)d\theta d\phi \quad . \quad (27)$$

In a slice of $360^\circ \times \Delta b$ the amount of solid angle, $\Delta\Omega$, is

$$\Delta\Omega = 2\pi((\cos(90^\circ) - \cos(b + \Delta b)) - (\cos(90^\circ) - \cos(b))) \text{ steradians} \quad . \quad (28)$$

The approximate number of galaxies in each slice can be found through the following approximation. Firstly, we find the largest value of the frequencies

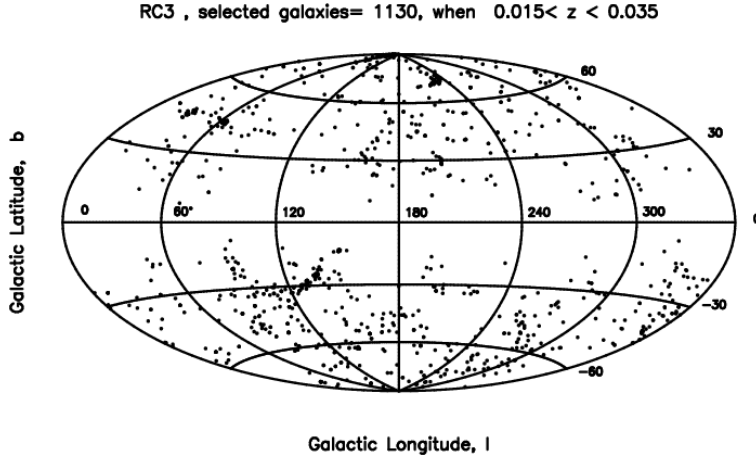


Figure 18: Hammer-Aitoff projection in galactic coordinates (observational counterpart of $V_s(2,3)$) of 1130 galaxies in the RC3 which have BT and $0.015 < z < 0.035$.

of galaxies, F_i , versus b , $max(F_i)$ where the index i denotes a class in latitude. We therefore find the largest value of $\Delta\Omega_i$, $max(\Delta\Omega_i)$. The introduction of the multiplicative factor M

$$M = \frac{max(F_i)}{max(\Delta\Omega_i)} \quad , \quad (29)$$

obtains the following theoretical evaluation of the number of galaxies N_i as a function of the latitude,

$$N_i = M \times \Delta\Omega_i \quad . \quad (30)$$

This number, N_i , as a function of b is plotted in Figure 19.

The simulation of this overall sky survey can be done in the following way:

- The pixels belonging to the faces of irregular polyhedron are selected according to the distribution in z of the galaxies in the RC3 catalog which have redshift and BT.

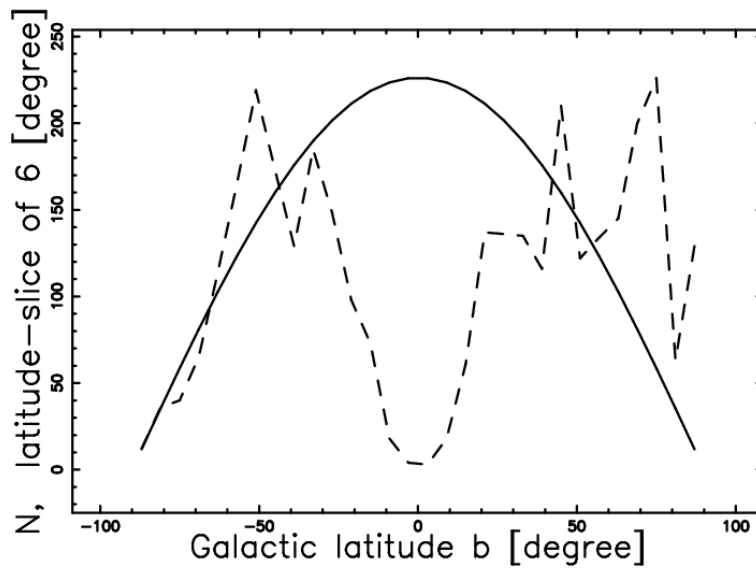


Figure 19: The galaxies in the RC3 which have BT and redshift are organized in frequencies versus galactic latitude b (dashed line). The theoretical fit represents N_i (full line).

Table 5: Real and Simulated data without the *Zone of Avoidance* in the RC3 catalog.

	<i>RC3</i>	<i>simulation without the Zone of Avoidance</i>
<i>elements</i>	3316	4326
z_{min}	5.7×10^{-7}	8.9×10^{-3}
$z_{pos-max}$	5.6×10^{-3}	8.9×10^{-2}
z_{ave}	1.52×10^{-2}	7.96×10^{-2}
z_{max}	9.4×10^{-2}	0.14

- A second operation selects the pixels according to the distribution in latitude in the RC3 catalog, see Figure 20.
- In order to simulate a theoretical distribution of objects which represent the RC3 catalog without the *Zone of Avoidance* we made a series of 6° slices in latitude in the RC3 catalog, selecting N_i pixels in each slice, see Figure 21. In order to ensure that the range in z is correctly described Table 5 reports z_{min} , $z_{pos-max}$, z_{ave} and z_{max} which represent the minimum z , the position in z of the maximum in the number of galaxies, and the maximum z in the RC3 catalog or the simulated sample.

5.3 The Eridanus Supervoid

A void can be defined as the empty space between filaments in a slice and the typical diameter has a range of $[11 - 50] Mpc/h$, see Einasto et al. (1994) and Lindner et al. (1995). The probability, for example, of having a volume 3 times bigger than the average is $3.2 \cdot 10^{-3}$ for PDF (23) when $d = 3$ and $2.1 \cdot 10^{-3}$ for PDF (22) when $d = 2.75$. Other values of the normalized volume are reported in Figure 11. Particularly large voids are called super-voids and have a range of $[110 - 163] Mpc/h$.

Special attention should be paid to the Eridanus super-void of $300 Mpc$ in diameter. This super-void was detected by the Wilkinson Microwave Anisotropy Probe (WMAP), see Vielva et al. (2004) Cruz et al. (2005) and

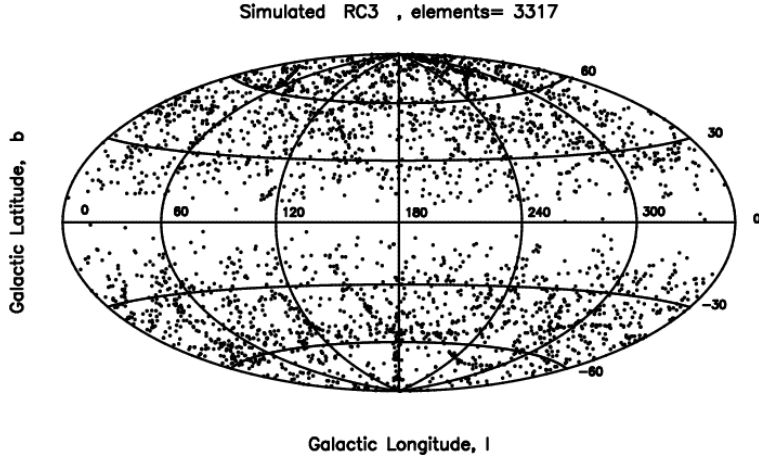


Figure 20: Hammer-Aitoff projection of 3317 pixels belonging to a face of an irregular Voronoi Polyhedron. The *Zone of Avoidance* at the galactic plane follows Figure 17. This plot simulates the RC3 galaxies which have BT and redshift.

was named *Cold Spot*. The WMAP measures the temperature fluctuations of the cosmic microwave background (CMB). Later on the radioastronomers confirmed the largest void due to the fact that the density of radio sources at 1.4 GHz is anomalously low in the direction of the *Cold Spot*, see Rudnick et al. (2007) and McEwen et al. (2008). The standard statistics of the Voronoi normalized volume distribution in 3D covers the range $[0.1 - 10]$. In the case of a Eridanus supervoid the normalized volume is $\approx \frac{300}{27} = 1.37 \cdot 10^3$ and the connected probability of having such a supervoid is $1.47 \cdot 10^{-18}$ when the Ferenc & Neda function with $d = 3$, formula (23), is used and ≈ 0 when the Kiang function with $d = 2.75$, formula (22) is used. Due to this low probability of having such a large normalized volume we mapped a possible spatial distribution of the SDSS-FIRST (the Faint Images of the Radio Sky at Twenty cm survey) sources with complex radio morphology from the theoretical distribution of galaxies belonging to the RC3. The fraction of galaxies belonging to the 2dFGRS detected as SDSS-FIRST sources with complex radio morphology is less than 10% according to Section 3.8 in Ivezić et al. (2002). We therefore introduced a probability, p_{rs} , that a galaxy is a

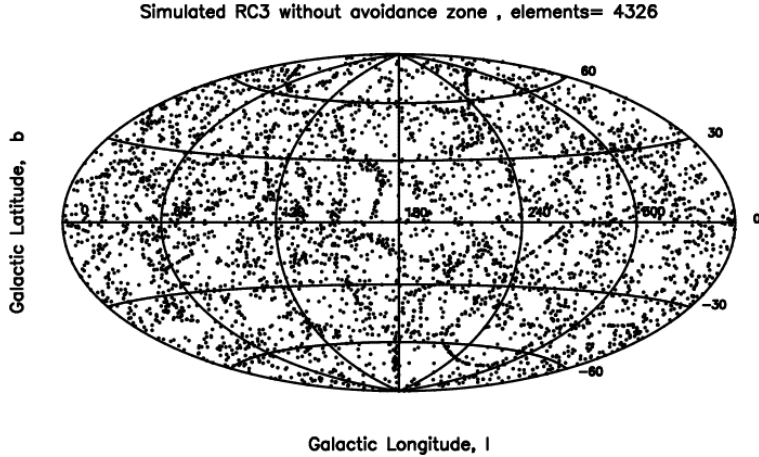


Figure 21: Hammer-Aitoff projection of 4326 pixels belonging to a face of an irregular Voronoi Polyhedron. This plot simulates the RC3 galaxies which have BT and redshift but the *Zone of Avoidance* at the galactic plane is absent.

radio source. The number of SDSS-FIRST sources N_{rs} in the RC3 which are SDSS-FIRST sources with complex radio morphology is

$$N_{rs} = p_{rs} * N_g \quad , \quad (31)$$

where N_g is the number of galaxies in the theoretical RC3.

From a visual inspection of Figure 21 and Figure 22 it is possible to conclude that the voids increase in size when radiogalaxies which are a subset of the galaxies are considered.

6 The correlation function for galaxies

Galaxies have the tendency to be grouped in clusters and a typical measure is the computation of the two-points correlation function for galaxies, see Peebles (1993, 1980). The correlation function can be computed in two ways: a local analysis in the range $[0 - 16]Mpc/h$ and an extended analysis in the range $[0 - 200]Mpc/h$.

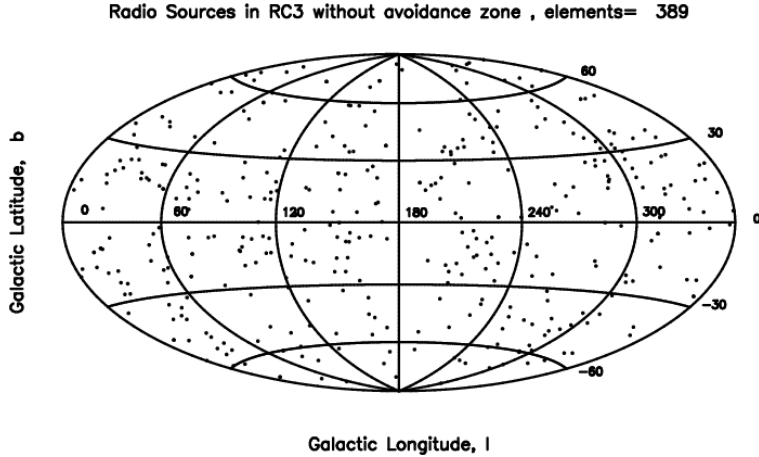


Figure 22: Hammer-Aitoff projection of the SDSS-FIRST sources with complex radio morphology belonging to the RC3, $p_{rs} = 0.09$. Other parameters as in Figure 21.

6.1 The local analysis

A first way to describe the degree of clustering of galaxies is the two point correlation function $\xi_{GG}(r)$, usually presented in the form

$$\xi_{GG} = \left(\frac{r}{r_G}\right)^{-\gamma_{GG}} \quad , \quad (32)$$

where $\gamma_{GG}=1.8$ and $r_G = 5.77h^{-1}Mpc$ (the correlation length) when the range $0.1h^{-1}Mpc < r < 16h^{-1}Mpc$ is considered, see Zehavi et al. (2004) where 118149 galaxies were analyzed.

In order to compute the correlation function, two volumes were compared: one containing the little cubes belonging to a face, the other containing a random distribution of points. From an analysis of the distances of pairs, the minimum and maximum were computed and $n_{DD}(r)$ was obtained, where $n_{DD}(r)$ is the number of pairs of galaxies with separation within the interval $[r - dr/2, r + dr/2]$. A similar procedure was applied to the random elements in the same volume with the same number of elements and $n_{RR}(r)$ is the number of pairs of the Poissonian Process. According to formula (16.4.6)

in Coles & Lucchin (2002) the correlation function is:

$$\xi_{GG}(r) = \frac{n_{DD}(r)}{n_{RR}(r)} - 1 \quad . \quad (33)$$

To check whether ξ_{GG} obeys a power law or not we used a simple linear regression test with the formula:

$$\text{Log } \xi_{GG} = a + b \text{ Log } r \quad , \quad (34)$$

which allows us to compute $r_G = 10^{-a/b}$ and $\gamma_{GG} = -b$.

We now outline the method that allow us to compute the correlation function using the concept of thick faces, see Zaninetti (1995). A practical implementation is to consider a decreasing probability of having a galaxy in the direction perpendicular to the face. As an example we assume a probability, $p(x)$, of having a galaxy outside the face distributed as a Normal (Gaussian) distribution

$$p(x) = \frac{1}{\sigma(2\pi)^{1/2}} \exp -\frac{x^2}{2\sigma^2} \quad , \quad (35)$$

where x is the distance in Mpc from the face and σ the standard deviation in Mpc . Once the complex 3D behavior of the faces of the Voronoi Polyhedron is set up we can memorize such a probability on a 3D grid $P(i, j, k)$ which can be found in the following way

- In each lattice point (i, j, k) we search for the nearest element belonging to a Voronoi face. The probability of having a galaxy is therefore computed according to formula (35).
- A number of galaxies, $N_G = n_* \times \text{side}^3$ is then inserted in the box; here n_* represents the density of galaxies

Figure 23 visualizes the edges belonging to the Voronoi diagrams and Figure 24 represents a cut in the middle of the probability, $P(i, j, k)$, of having a galaxy to a given distance from a face.

A typical result of the simulation is reported in Figure 25 where the center of the smaller box in which the correlation function is computed is the point belonging to a face nearest to the center of the big box.

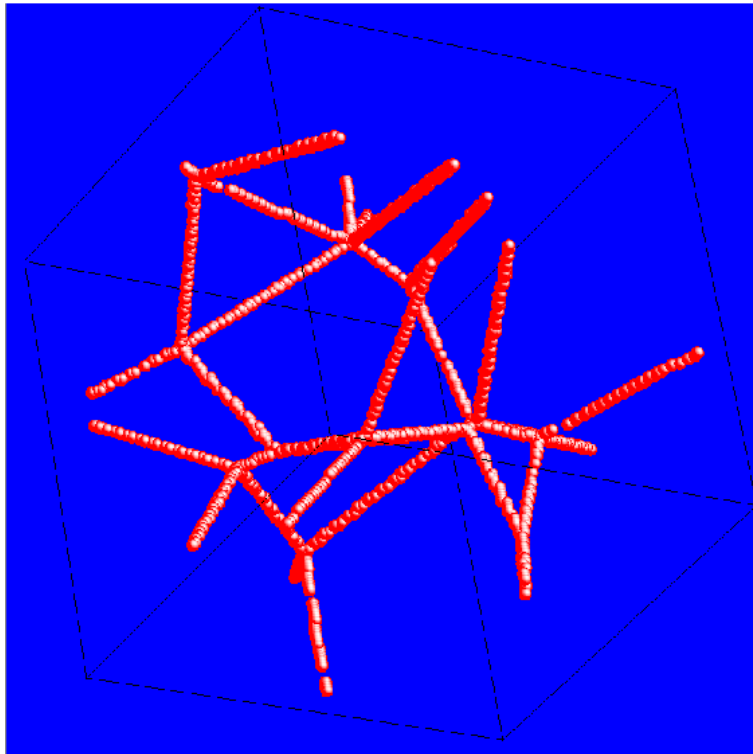


Figure 23: 3D visualization of the edges of the Poissonian Voronoi–diagram. The parameters are $pixels=60$, $N_s=12$, $side=96.24\text{ Mpc}$, $h=0.623$ and $amplify=1.2$.

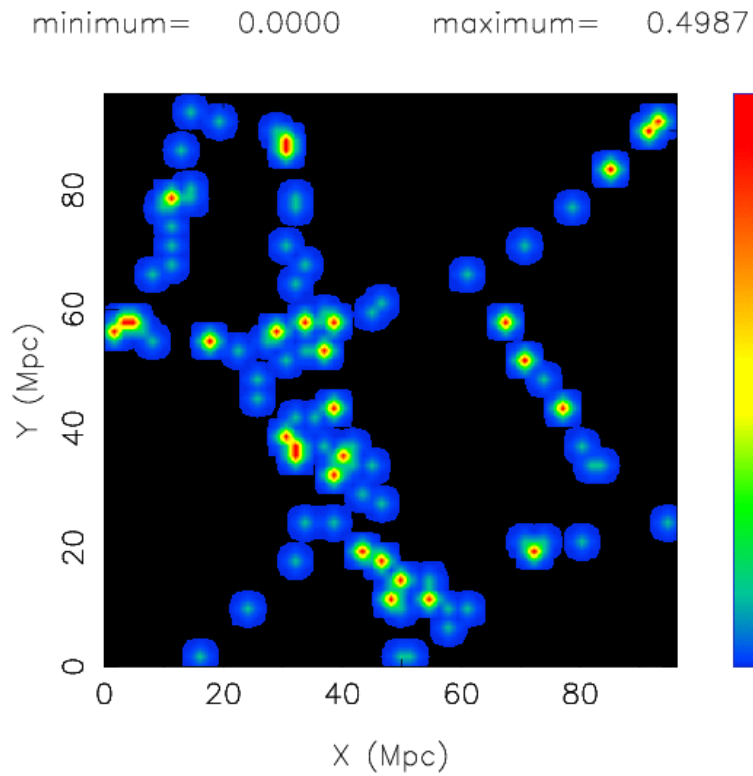


Figure 24: Cut in the middle of the 3D grid $P(i, j, k)$ which represents a theoretical 2D map of the probability of having a galaxy. The Voronoi parameters are the same as in Figure 23 and $\sigma = 0.8Mpc$. The X and Y units are in Mpc.

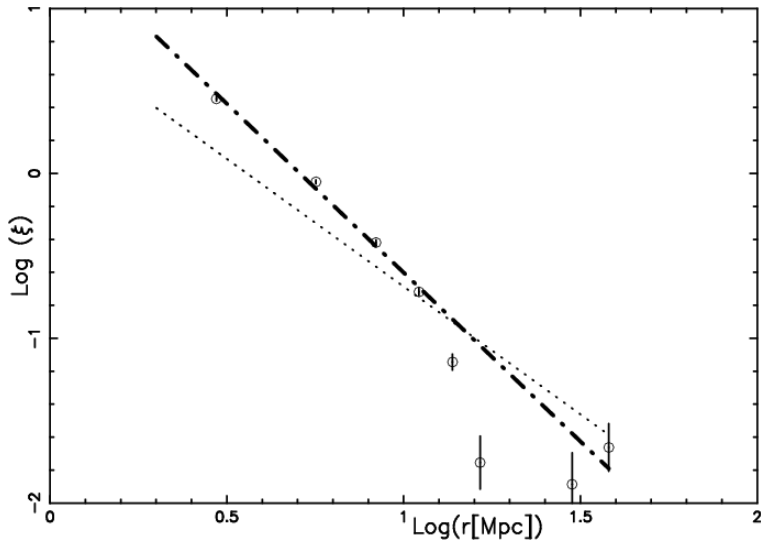


Figure 25: The logarithm of the correlation function is visualized through points with their uncertainty (vertical bar), the asymptotic behavior of the correlation function ξ_{GG} is reported as dash-dot-dash line; in our simulation $\gamma_{GG}=2.04$ and $r_G = 5.08$ Mpc. The standard value of the correlation function is reported as a dotted line; from the point of view of the observations in average $\gamma_{GG}=1.8$ and $r_G = 5$ Mpc. Parameters of the simulation as in Figure 23.

From an analysis of Figure 25 we can deduce that the correlation function ξ_{GG} of the simulation has a behavior similar to the standard one. Perhaps the value r_G is a simple measure of the face's thickness, ΔR_F . From this point of view on adopting a standard value of the expanding shell thickness, $\Delta R = \frac{R}{12}$ and assuming that the thickness of the shell is made by the superposition of two expanding shells the following is obtained

$$\Delta R_F \approx \frac{R}{6} \approx \frac{\overline{D^{obs}}}{h 12} = 3.62 \text{ Mpc} \quad , \quad (36)$$

where $h = 0.623$ has been used. The correlation dimension D_2 , see Jones et al. (2005), is connected with the exponent γ through the relation:

$$D_2 = 3 - \gamma \quad . \quad (37)$$

Here there is the case in which the mass $M(r)$ increases as $r^{1.2}$, in the middle of a one dimensional structure ($M(r) \propto r$) and a two dimensional sheet ($M(r) \propto r^2$), see Coles & Lucchin (2002). In this paragraph the dependence of the correlation function on the magnitude is not considered.

6.2 The extended analysis

A second definition of the correlation function takes account of the Landy-Szalay border correction, see Szalay et al. (1993),

$$\xi_{LS}(s) = 1 + \frac{n_{DD}(s)}{n_{RR}(s)} - 2 \frac{n_{DR}(s)}{n_{RR}(s)} \quad . \quad (38)$$

where $n_{DD}(s)$, $n_{DD}(s)$ and $n_{DR}(s)$ are the number of galaxy-galaxy, random-random and galaxy-random pairs having distance s , see Martínez et al. (2009). A random catalog of galaxies in polar coordinates can be built by generating a first random number $\propto z^2$ in the z -space and a second random angle in the interval $[0, 75]$. A test of our code for the correlation function versus a more sophisticated code is reported in Figure 26 for the 2dFVL volume limited (VL) sample, where the data available at the Web site <http://www.uv.es/martinez/> have been processed.

The pair correlation function for the vertexes of the Poissonian Voronoi Polyhedron presents a typical damped oscillation, see Figure 5.4.11 in Okabe et al. (1992), Figure 2 in Martínez et al. (2009) and Figure 3 in Heinrich

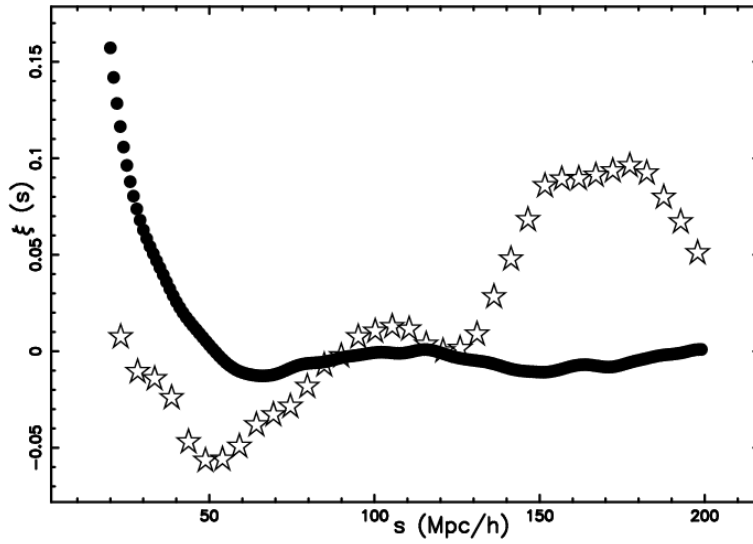


Figure 26: Redshift-space correlation function for the 2dFGRS sample limited at $z = 0.12$ as given by our code (empty stars) and the results of Martínez et al. (2009) (full points) for 2dFVL. The covered range is $[40 - 200]Mpc/h$.

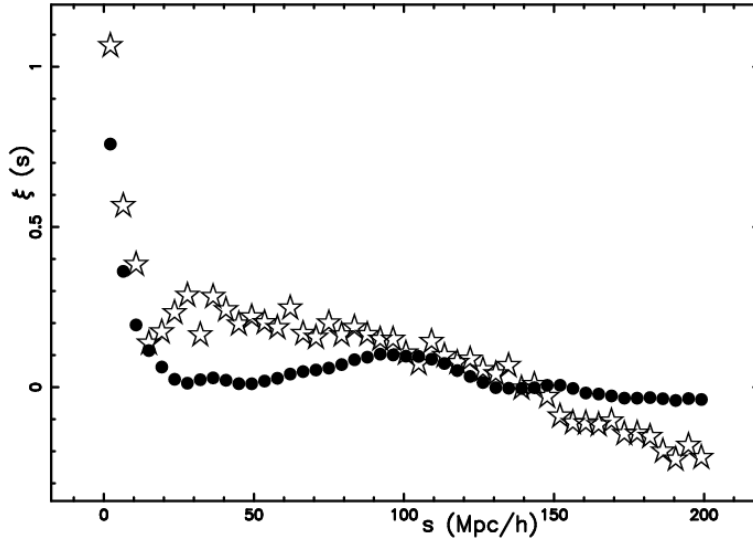


Figure 27: Redshift-space correlation function for the 2dfGRS sample (empty stars) and the Voronoi sample(full points). The covered range is $[40 - 200]Mpc/h$.

& Muche (2008). Here conversely : (a) we first consider a set of objects belonging to the faces of the irregular Polyhedron ; (b) we extract from the previous set a subset which follows the photometric law and then we compute the pair correlation function. The difference between our model and the model in Martínez et al. (2009) for 2dFVL can be due to the luminosity color segregation presents in 2dFVL but not in our Voronoi type model. A typical result is reported in Figure 27 where it is possible to find the correlation function of 2dfGRS with astronomical data as reported in Figure 13 as well as the correlation function of the Voronoi network with simulated data as reported in Figure 15.

A careful analysis of Figure 27 allows us to conclude that the behavior of the correlation function is similar for the astronomical data as well as the simulated Voronoi-data. The oscillations after $100 Mpc$ are classified as acoustic, Eisenstein et al. (2005).

7 Summary

Photometric maximum

The observed number of galaxies in a given solid angle with a chosen flux/magnitude versus the redshift presents a maximum that is a function of the flux/magnitude. From a theoretical point of view, the photometric properties of the galaxies depend on the chosen law for the luminosity function. The luminosity function here adopted (the Schechter function) predicts a maximum in the theoretical number of galaxies as a function of the redshift once the apparent flux/magnitude is fixed.

The theoretical fit representing the number of galaxies as a function of the redshift can be compared with the real number of galaxies of the 2dFGRS which is theory-independent. The superposition of theoretical and observed fit is satisfactory and the χ^2 has been computed, see Figure 1. The position of the maximum in the number of galaxies for different magnitudes is a function of the redshift and in the interval $15 < bJmag < 18.5$ the comparison between observed and theoretical data is acceptable, see Figure 3. Particular attention should be paid to the Malmquist bias and to equation (15) that regulate the upper value of the redshift that defines the complete sample.

3D Voronoi Diagrams The intersection between a plane and the 3D Voronoi faces is well known as $V_p(2, 3)$. The intersection between a slice of a given opening angle, for example 3° , and the 3D Voronoi faces is less known and has been developed in Section 4.2. This intersection can be calibrated on the astronomical data once the number of Poissonian seeds is such that the largest observed void matches the largest Voronoi volume. Here the largest observed void is 2700 Km/sec and in order to simulate, for example, the 2dFGRS, 137998 Poissonian seeds were inserted in a volume of $(131908 \text{ Km/sec})^3$. The intersection between a sphere and the 3D Voronoi faces represents a new way to visualize the voids in the distribution of galaxies, see Section 4.2. In this spherical cut the intersection between a sphere and the 3D Voronoi faces is no longer represented by straight lines but by curved lines presenting in some cases a cusp behavior at the intersection, see Figure 7. In line of principle the spatial distribution of galaxies at a given redshift should follow such curved lines.

Statistics of the voids The statistical properties of the voids between galaxies can be well described by the volume distribution of the Voronoi Polyhedra. Here two distributions of probability were carefully compared: the old Kiang

function here parametrized as a function of the dimension d , see formula (21), and the new distribution of Ferenc & Neda, see formula (23), which is a function of the selected dimension d . The probability of having voids as large as the Eridanus super-void was computed, see Section 5.3.

Simulations of the catalogs of galaxies By combining the photometric dependence in the number of galaxies as a function of the redshift with the intersection between a slice and the Voronoi faces, it is possible to simulate the astronomical catalogs such as the 2dFGRS, see Section 5.1. Other catalogs such as the RC3 which covers all the sky (except the Zone of Avoidance) can be simulated through a given number of spherical cuts, for example 25, with progressive increasing redshift. This simulation is visible in Figure 20 in which the theoretical influence of the Zone of Avoidance has been inserted, and in Figure 21 in which the theoretical RC3 without the Zone of Avoidance has been modeled. Figure 22 reports the subset of the galaxies which are radiogalaxies.

Correlation function The standard behavior of the correlation function for galaxies in the short range $[0-10 \text{ Mpc}/h]$ can be simulated once 12 Poissonian seeds are inserted in a box of volume $(96.24 \text{ Mpc}/h)^3$. In this case the model can be refined by introducing the concept of galaxies generated in a thick face belonging to the Voronoi Polyhedron. The behavior of the correlation function in the large range $[40-200 \text{ Mpc}/h]$ of the Voronoi simulations of the 2dFGRS presents minimum variations from the processed astronomical data, see Figure 27. We now extract a question from the conclusions of Martínez et al. (2009) “Third, the minimum in the large-distance correlation functions of some samples demands explanation: is it really the signature of voids?” Our answer is “yes”. The minimum in the large scale correlation function is due to the combined effect of the large empty space between galaxies (the voids) and to the photometric behavior of the number of galaxies as a function of the red-shift.

A The maximum likelihood estimator

The parameter \hat{z}_{crit} can be derived through the maximum likelihood estimator (MLE) and as a consequence $z = z_{pos-max}$ is easily derived. The likelihood function is defined as the probability to obtain a set of observations if given

particular set of the distribution parameters, c_i ,

$$L(c) = f(x_1 \dots x_n | c_1 \dots c_n) \quad . \quad (\text{A.1})$$

If we assume that the n random variables are independently and identically distributed, then we may write the likelihood function as

$$L(c) = f(x_1 | c_1 \dots c_p) \dots f(x_n | c_1 \dots c_p) = \prod_{i=1}^n f(x_i | c_1 \dots c_p) \quad . \quad (\text{A.2})$$

The maximum likelihood estimates for the c_i are obtained by maximizing the likelihood function, $L(c)$. In the same way, we may find it easier to maximize $\ln f(x_i)$, termed the log-likelihood. So, for a random sample $z_1 \dots z_n$ representing the redshift of the galaxies that fall in a given interval of flux or magnitude from a joint distribution in z and f for galaxies adopting the Schechter function for the luminosity represented by equation (3), the likelihood function is given by

$$L(z_{crit}) = \prod_{i=1}^n (z_i)^{2\alpha+4} \frac{1}{(z_{crit})^{2\alpha}} \exp -\frac{z_i^2}{z_{crit}^2} \quad , \quad (\text{A.3})$$

where the constant terms are omitted. Using logarithms, we obtain the log-likelihood

$$\ln L(z_{crit}) = (2\alpha + 4) \sum_{i=1}^n \ln z_i + n2 | \alpha | \ln(z_{crit}) - \sum_{i=1}^n \frac{z_i^2}{z_{crit}^2} \quad . \quad (\text{A.4})$$

Taking the first derivative with respect to z_{crit} equal to zero, we get

$$\hat{z}_{crit} = \sqrt{\frac{\sum_{i=1}^n z_i^2}{n | \alpha |}} \quad . \quad (\text{A.5})$$

According to equation (6) $\hat{z}_{pos-max}$ is

$$\hat{z}_{pos-max} = \sqrt{\frac{\sum_{i=1}^n z_i^2}{n | \alpha |}} \sqrt{\alpha + 2} \quad (\text{A.6})$$

When a joint distribution in z and f for galaxies in the presence of the $\mathcal{M} - L$ relationship is considered, see equation (38) in Zaninetti (2008), the likelihood function is

$$L(z_{crit}) = \prod_{i=1}^n (z_i)^{4+2\frac{c-a}{a}} (z_{crit})^{-2\frac{c-a}{a}} \exp -\left(\frac{z_i^2}{z_{crit}^2}\right)^{1/a} \quad , \quad (\text{A.7})$$

where the constant terms are omitted. Taking the first derivative with respect to z_{crit} of $\ln L(z_{crit})$ equal to zero, we get for the $\mathcal{M} - L$ relationship

$$\hat{z}_{crit} = \left(\frac{\sum_{i=1}^n z_i^{2/a}}{n |c - a|} \right)^{a/2} . \quad (\text{A.8})$$

According to equation (10) $\hat{z}_{pos-max}$ for the $\mathcal{M} - L$ relationship is

$$\hat{z}_{pos-max} = \left(\frac{\sum_{i=1}^n z_i^{2/a}}{n |c - a|} \right)^{a/2} (a + c)^{a/2} . \quad (\text{A.9})$$

Acknowledgements

I thank the 2dF Galaxy Redshift Survey team for the use of Figure 14, which is taken from the image gallery on the 2dFGRS website (see <http://www2.aao.gov.au/2dFGRS>).

References

- Aarseth, S. J. 1978, in *The large scale structure of the universe*, p. 189 - 196, 189–196
- Barrow, J. D. & Coles, P. : 1990, *MNRAS* , **244**, 188
- Behr, A. : 1951, *Astronomische Nachrichten*, **279**, 97
- Berlind, A. A., Frieman, J., Weinberg, D. H., & et al. : 2006, *ApJS* , **167**, 1
- Bernardeau, F. & van de Weygaert, R. : 1996, *MNRAS* , **279**, 693
- Charlton, J. C. & Schramm, D. N. : 1986, *ApJ* , **310**, 26
- Coles, P. : 1991, *Nature* , **349**, 288
- Coles, P. & Lucchin, F. : 2002, *Cosmology: The Origin and Evolution of Cosmic Structure*, Second Edition (Chichester, England: John Wiley & Son)
- Colless, M., Dalton, G., Maddox, S., & et al. : 2001, *MNRAS* , **328**, 1039

- Cooray, A. & Sheth, R. : 2002, Phys. Rep. , **372**, 1
- Cruz, M., Martínez-González, E., Vielva, P., & Cayón, L. : 2005, MNRAS , **356**, 29
- de Vaucouleurs, G., de Vaucouleurs, A., Corwin, Jr., H. G., et al. : 1991, Third Reference Catalogue of Bright Galaxies (New York, NY: Springer-Verlag)
- Ebeling, H. & Wiedenmann, G. : 1993, Phys. Rev. E , **47**, 704
- Einasto, M., Einasto, J., Tago, E., Dalton, G. B., & Andernach, H. : 1994, MNRAS , **269**, 301
- Eisenstein, D. J., Zehavi, I., Hogg, D. W., et al. : 2005, ApJ , **633**, 560
- Eke, V. R., Frenk, C. S., Baugh, C. M., Cole, S., & Norberg, P. : 2004, MNRAS , **355**, 769
- Elyiv, A., Melnyk, O., & Vavilova, I. : 2009, MNRAS , **394**, 1409
- Evrard, A. E., MacFarland, T. J., Couchman, H. M. P., et al. : 2002, ApJ , **573**, 7
- Ferenc, J.-S. & Néda, Z. : 2007, Phys. A , **385**, 518
- Geller, M. J. & Huchra, J. P. : 1989, Science, **246**, 897
- Goldwirth, D. S., da Costa, L. N., & van de Weygaert, R. : 1995, MNRAS , **275**, 1185
- Gott, III, J. R. & Rees, M. J. : 1975, A&A , **45**, 365
- Gott, III, J. R., Turner, E. L., & Aarseth, S. J. : 1979, ApJ , **234**, 13
- Heinrich, L. & Mücke, L. : 2008, Math. Nachr., **281**, 350
- Hubble, E. : 1929, Proceedings of the National Academy of Science, **15**, 168
- Icke, V. & van de Weygaert , R. : 1987, A&A , **184**, 16
- Ikeuchi, S. & Turner, E. L. : 1991, MNRAS , **250**, 519

- Ivezić, Ž., Menou, K., Knapp, G. R., Strauss, M. A., & Lupton, R. H. : 2002, *AJ* , **124**, 2364
- Jones, B. J., Martínez, V. J., Saar, E., & Trimble, V. : 2005, *Rev. Mod. Phys.* , **76**, 1211
- Kiang, T. : 1966, *Z. Astrophys.* , **64**, 433
- Klypin, A. & Shandarin, S. F. : 1993, *ApJ* , **413**, 48
- Lindner, U., Einasto, J., Einasto, M., et al. : 1995, *A&A* , **301**, 329
- Madgwick, D. S., Lahav, O., Baldry, I. K., et al. : 2002, *MNRAS* , **333**, 133
- Malmquist , K. : 1920, *Lund Medd. Ser. II*, **22**, 1
- Malmquist , K. : 1922, *Lund Medd. Ser. I*, **100**, 1
- Mandelbrot, B. : 1975, *Academie des Sciences Paris Comptes Rendus Serie Sciences Mathematiques*, **280**, 1551
- Marinoni, C., Davis, M., Newman, J. A., & Coil, A. L. : 2002, *ApJ* , **580**, 122
- Martínez, V. J., Arnalte-Mur, P., Saar, E., et al. : 2009, *ApJ* , **696**, L93
- McEwen, J. D., Wiaux, Y., Hobson, M. P., Vandergheynst, P., & Lasenby, A. N. : 2008, *MNRAS* , **384**, 1289
- Melnyk, O. V., Elyiv, A. A., & Vavilova, I. B. : 2006, *Kinematika i Fizika Nebesnykh Tel*, **22**, 283
- Neyman, J. & Scott, E. L. : 1952, *ApJ* , **116**, 144
- Neyrinck, M. C., Gnedin, N. Y., & Hamilton, A. J. S. : 2005, *MNRAS* , **356**, 1222
- Okabe, A., Boots, B., & Sugihara, K. : 1992, *Spatial tessellations. Concepts and Applications of Voronoi diagrams* (Chichester, New York: Wiley)
- Padmanabhan, P. : 2002, *Theoretical astrophysics. Vol. III: Galaxies and Cosmology* (Cambridge, MA: Cambridge University Press)

- Padmanabhan, T. : 1996, *Cosmology and Astrophysics through Problems* (Cambridge: Cambridge University Press)
- Peebles, P. J. E. : 1974a, *Astrophysics and Space Science* , **31**, 403
- Peebles, P. J. E. : 1974b, *ApJ* , **189**, L51+
- Peebles, P. J. E. : 1980, *The large-scale structure of the universe* (Princeton, N.J.: Princeton University Press)
- Peebles, P. J. E. : 1993, *Principles of physical cosmology* (Princeton, N.J.: Princeton University Press)
- Pierre, M. : 1990, *A&A* , **229**, 7
- Press, W. H., Teukolsky, S. A., Vetterling, W. T., & Flannery, B. P. : 1992, *Numerical recipes in FORTRAN. The art of scientific computing* (Cambridge: Cambridge University Press)
- Rudnick, L., Brown, S., & Williams, L. R. : 2007, *ApJ* , **671**, 40
- Sahni, V. & Coles, P. : 1995, *Phys. Rep.* , **262**, 1
- Sandage, A., Tammann, G. A., Saha, A., et al. : 2006, *ApJ* , **653**, 843
- Schaap, W. E. & van de Weygaert, R. : 2000, *A&A* , **363**, L29
- Schechter, P. : 1976, *ApJ* , **203**, 297
- Scherrer, R. J. & Bertschinger, E. : 1991, *ApJ* , **381**, 349
- Shandarin, S. F. & Zel'dovich , Y. B. : 1989, *Rev. Mod. Phys.* , **61**, 185
- Soneira, R. M. & Peebles, P. J. E. : 1977, *ApJ* , **211**, 1
- Soneira, R. M. & Peebles, P. J. E. : 1978, *AJ* , **83**, 845
- Sparke, L. S. & Gallagher, III, J. S. : 2000, *Galaxies in the universe : an introduction* (Cambridge, UK: Cambridge University Press)
- Subba Rao, M. U. & Szalay, A. S. : 1992, *ApJ* , **391**, 483

- Szalay, A. S., Broadhurst, T. J., Ellman, N., Koo, D. C., & Ellis, R. S. : 1993, Proceedings of the National Academy of Science, **90**, 4853
- Tempel, E., Einasto, J., Einasto, M., Saar, E., & Tago, E. : 2009, A&A , **495**, 37
- Turner, E. L., Aarseth, S. J., Blanchard, N. T., Mathieu, R. D., & Gott, III, J. R. : 1979, ApJ , **228**, 684
- van de Weygaert , R. : 1991, MNRAS , **249**, 159
- van de Weygaert, R. : 1991, Ph.D. thesis, University of Leiden
- van de Weygaert, R. : 2002, arXiv:astro-ph/0206427
- van de Weygaert, R. 2003, Statistics of Galaxy Clustering - Commentary (Statistical Challenges in Astronomy), 156–186
- van de Weygaert, R. & Icke, V. : 1989, A&A , **213**, 1
- van de Weygaert, R. & Schaap, W. 2009, in Lecture Notes in Physics, Berlin Springer Verlag, Vol. 665, Lecture Notes in Physics, Berlin Springer Verlag, ed. V. J. Martinez, E. Saar, E. M. Gonzales, & M. J. Pons-Borderia , 291–+
- Vielva, P., Martínez-González, E., Barreiro, R. B., Sanz, J. L., & Cayón, L. : 2004, ApJ , **609**, 22
- von Benda-Beckmann, A. M. & Müller, V. : 2008, MNRAS , **384**, 1189
- Zaninetti, L. : 1995, A&AS , **109**, 71
- Zaninetti, L. : 2006, Chinese J. Astron. Astrophys. , **6**, 387
- Zaninetti, L. : 2008, AJ , **135**, 1264
- Zaninetti, L. & Ferraro, M. : 1990, A&A , **239**, 1
- Zehavi, I., Weinberg, D. H., Zheng, Z., et al. : 2004, ApJ , **608**, 16
- Zel'dovich , Y. B. : 1970, A&A , **5**, 84